Accepted Manuscript

Structure-guided discovery of thiazolidine-2,4-dione derivatives as a novel class of *Leishmania major* pteridine reductase 1 inhibitors

Franco Henrique A. Leite, Priscila Brandão Gomes da Silva Santiago, Thamires Quadros Froes, João da Silva Filho, Suellen Gonçalves da Silva, Rafael M. Ximenes, Antônio Rodolfo de Faria, Dalci José Brondani, Julianna F.C. de Albuquerque, Marcelo Santos Castilho

PII: S0223-5234(16)30623-7

DOI: 10.1016/j.ejmech.2016.07.060

Reference: EJMECH 8778

To appear in: *European Journal of Medicinal Chemistry*

Received Date: 30 January 2016

Revised Date: 20 July 2016

Accepted Date: 24 July 2016

Please cite this article as: F.H.A. Leite, P.B.G.d.S. Santiago, T.Q. Froes, J. da Silva Filho, S.G. da Silva, R.M. Ximenes, A.R. de Faria, D.J. Brondani, J.F.C. de Albuquerque, M.S. Castilho, Structure-guided discovery of thiazolidine-2,4-dione derivatives as a novel class of *Leishmania major* pteridine reductase 1 inhibitors, *European Journal of Medicinal Chemistry* (2016), doi: 10.1016/j.ejmech.2016.07.060.

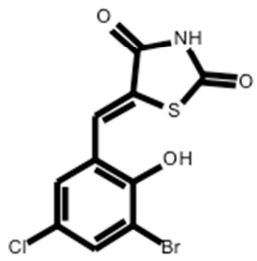

IC_{50}= 44.67± 1.74 µM

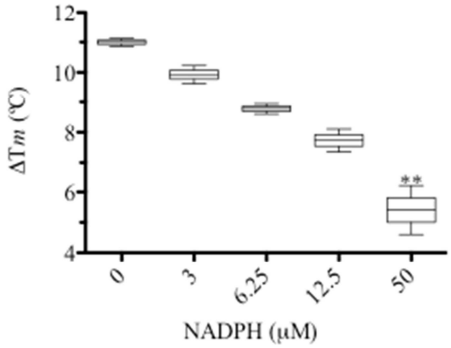

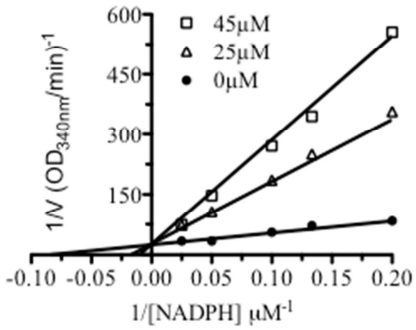

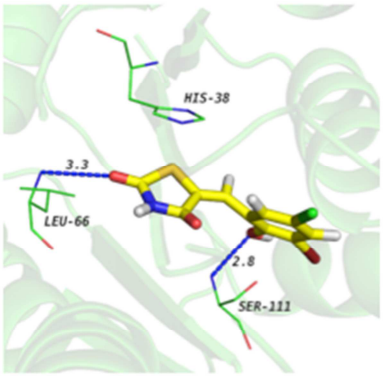

Structure-guided lead identification protocol

Structure-guided discovery of thiazolidine-2,4-dione derivatives as a novel class of *Leishmania major* Pteridine Reductase 1 inhibitors

Franco Henrique A. Leite[a], Priscila Brandão Gomes da Silva Santiago[b], Thamires Quadros Froes[d], João da Silva Filho[b], Suellen Gonçalves da Silva[d], Rafael M. Ximenes[b], Antônio Rodolfo de Faria[c], Dalci José Brondani[c], Julianna F. C. de Albuquerque[b], Marcelo Santos Castilho[a,d,*]

[a]Programa de Pós-graduação em Biotecnologia – PPGBiotec, Universidade Estadual de Feira de Santana; (Brasil) [b]Departamento de Antibióticos, Universidade Federal de Pernambuco (Brasil), [c]Departamento de Farmácia da Universidade Federal de Pernambuco (Brasil), [d]Faculdade de Farmácia da Universidade Federal da Bahia (Brasil).

*Corresponding author.
E-mail address: castilho@ufba.br (M. S. Castilho)

Abstract – *Leishmania major*, as other protozoan parasites, plague human kind since pre-historic times but it remains a worldwide ailment for which the therapeutic arsenal remains scarce. Although *L. major* is pteridine- and purine- auxotroph, well-established folate biosynthesis inhibitors, such as methotrexate, have poor effect over the parasite survival. The lack of efficiency is related to an alternative biochemical pathway in which pteridine reductase 1 (PTR1) plays a major role. For this reason, this enzyme has been considered a promising target for anti-leishmanial drug development and several inhibitors that share the substrate scaffold have been reported. In order to design a novel class of PTR1 inhibitors, we employed the thiazolidinone ring as a bioisosteric replacement for pteridine/purine ring. Among seven novel thiazolidine-2,4-dione derivatives reported herein, **2d** was identified as the most promising lead by thermal shift assays (ΔTm= 11 ºC, p= 0,01). Kinetic assays reveal that **2d** has IC50 = 44.67± 1.74 μM and shows a noncompetitive behavior. This information guided docking studies and molecular dynamics simulations (50000 ps) that supports **2d** putative binding profile (H-bonding to Ser-111 and Leu-66) and shall be useful to design more potent inhibitors.

Keywords: Leishmania; Thiazolidine-2,4-dione derivatives; Pteridine Reductase 1; Thermal shift assay; Kinetic assay; Molecular modeling.

Highlights

- Thiazolidine-2,4-dione derivatives are promising leads for antileishmanial drug design.
- Thiazolidinone ring mimics NADPH binding, thus acting as a noncompetitive inhibitor.
- Molecular dynamics support thiazolidine-2,4-dione one binding profile to LmPTR1.

1. Introduction

Neglected tropical diseases pose a threat to human health and welfare around the world, but drug development against such ailments remains slow [1]. Leishmaniasis, for instance, is rated the second most important disease caused by protozoans, thus being responsible for more than 20000 deaths annually [2]. However, the therapeutic arsenal available for its treatment is limited to a few drugs that have low efficacy and poor safety profile [3]. In order to modify this scenario synthetic efforts have been made to find promising lead compounds against *L. major* [4,5] and validated targets have been pursued [6]. Among them, folate metabolism is considered quite promising due to the fact that Leishmania as well as other tripanossomatides are pteridine auxotrophs [7,8]. Accordingly Tetrahydrofolate (H4-folate) and pterin, in its reduced form (H4-pterin), are essential cofactors for thymidine biosynthesis [9].

In Leishmania parasites, H4-folate is generated from folate and/or dihydrofolate (H2-folate) by the NADPH-dependent enzyme Dihydrofolate Reductase (DHFR), which also catalyzes the conversion of Deoxyuridine monophosphate (dUMP) to Deoxythymidine Monophosphate (dTMP), thus it acts as a thymidilate synthase (TS) and hence it is usually known as DHFR-TS [10]. Although the inhibition of either reaction should limit the supply of dTMP for DNA synthesis [11], DHFR inhibitors are ineffective against *Leishmania major* [12]. This unsettling result was clarified by the discovery of Pteridine Reductase 1 (PTR1), which guarantees the necessary amounts of folate, when *L. major* DHFR-TS is inhibited [13] (Fig. 1).

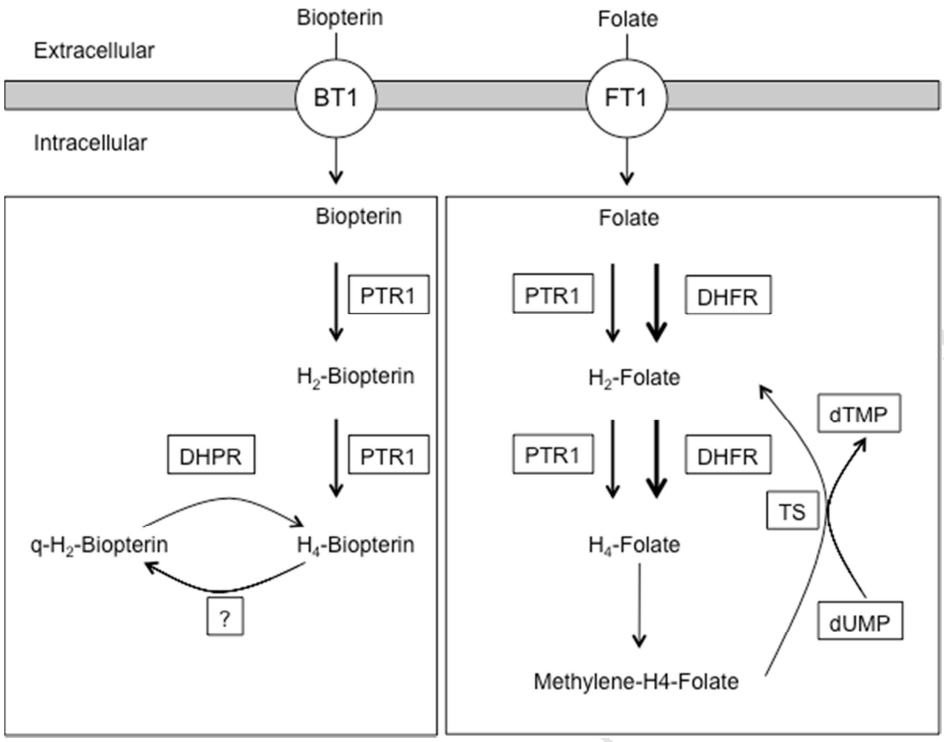

Fig. 1. Pteridine salvage pathway in Leishmania [7]. BT1, biopterin transporter 1; FT1, folate transporter 1; H_2-Biopterin, dihydrobiopterin; H_4-Biopterin, tetrahydrobiopterin; H_2-Folate, dihydrofolate; H_4-Folate, tetrahydrofolate; PTR1, pteridine reductase 1; DHFR, bifunctional dihydrofolate reductase-thymidylate synthase; DHPR, dihydropteridine reductase; q-H_2-biopterin, quinonoid dihydrobiopterin; '?', unknown enzyme(s). The widths of the arrows relate to their importance when more than one enzyme is responsible for the biochemical step.

Recently, it has been shown that PTR1 blockage can be deadly to *L. major*, once LmDHFR-TS is unable to reduce unconjugated pteridines [11]. Furthermore, this enzyme is not present in mammalian hosts rendering it a promising target for drug development. Most efforts towards this goal have relied on the design of 2-4-diamino purine derivatives that mimic the pteridine ring [14,15,16]. The work presented here takes an alternative route and builds on the previous knowledge that thiazolidinone ring might bind in the same way as the purine ring in some

macromolecular targets [17]. Another advantage of this class it that several thiazolidine-2,4-dione derivatives can be obtained by substitution on the heterocyclic ring making it possible to investigate structure-activity relationships [18]. This approach has already led to compounds with cardiotonic [19] anticancer [20,21], anticonvulsant [22] anti-inflammatory [23], antidiabetic [24,25], and antimicrobial [26,27,28] activity. Following this trend, a series of thiazolidine-2,4-dione derivatives was synthetized and screened against LmPTR1 through thermal shift assays (TSA) and the most promising molecule (**2d**) had its inhibition mechanism confirmed by two different approaches (TSA and kinetic studies). These *in vitro* results support our initial planning and guided docking and molecular dynamic studies that shed some light on the binding profile of this novel class of LmPTR1 inhibitors.

2. Results and discussion

2.1 Chemistry

The compounds **(2a-g)** were synthesized by Knoevenagel condensation with seven aromatic aldehydes yielding 5-arylidene-thiazolidine-2,4-dione derivatives, as outlined in Scheme 1. Thiazolidine-2,4-dione (**1**) was prepared according to the literature [29,30]. The structures of the final compounds were confirmed by ^{1}H NMR, ^{13}C NMR, IR, and mass spectrometry. The infrared spectrum of these compounds shows a strong absorption band between 3178 at 3157 cm^{-1} (N-H absorption) and 1773-1669 cm^{-1} (carbonyl in positions 2 and 4 of the thiazolidine-2,4-dione ring). The thiazolidin-2,4-dione derivatives might be produced as *E* or *Z* isomers, according to the literature [31], but only the *Z* isomers were found in this work, as suggested by thiazolidinone ring methylenic proton NMR absorption: All compounds have singlets between 7.77 and 7.79 ppm. This result agrees with previous studies in which imidazolidine-2,4-dione ring condensation with aromatic aldehydes, in an acid medium, led only to the *Z* isomer [31,32].

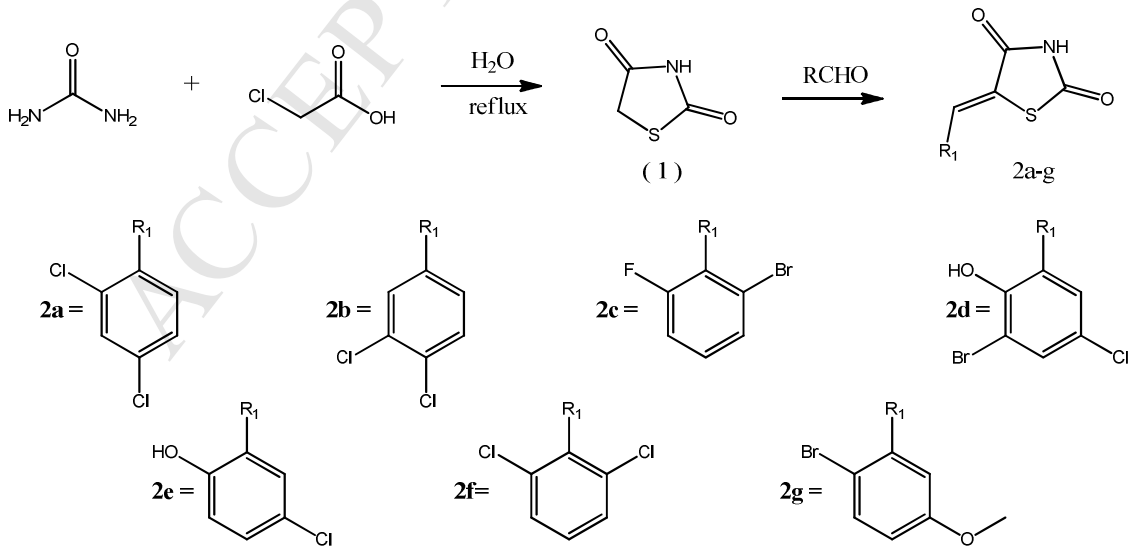

Scheme 1. Synthetic routes for the series of thiazolidine-2,4-dione derivatives.

The ^{1}H NMR spectra of compounds **2d** and **2e** presented an additional singlet at 6.07 ppm (OH absorption) whereas **2g** shows a singlet at 3.65 ppm (OCH_3 absorption). Among the seven final compounds, four have not been described before. Complete data concerning the physicochemical properties of all the synthesized compounds, (**1** and **2a-g**), are summarized in the experimental section of this study.

2.2 In vitro assays

2.2.1 TSA optimization

As mentioned before, we hypothesized that thiazolidine-2,4-dione derivatives might mimic either the substrate 2,4 pteridine ring (competitive behavior) or the cofactor purine ring (noncompetitive behavior). However, setting a kinetic assay that favors the discovery of competitive inhibitors over noncompetitive inhibitors, or vice-versa, might be misleading as there in no way to foresee which one will progress more swiftly through drug development steps. Although a balanced assay is commonly employed to circumvent this drawback, compounds that absorb light in the 340 nm range cannot be assayed against LmPTR1. Thermal shift assays (TSA), also known as ThermoFluor® assay, have been employed as a cheap, HTS-friendly alternative that relies on the thermodynamic principle of protein stabilization due to ligand binding [33]. Although this technique has been largely employed in screening campaigns, its sensible use requires the optimization of several parameters, such as the concentration of protein that affords optimal signal to noise ratio (quantum yield), pH/DMSO compatibility and so forth. Although 2 μM protein solutions can be

employed for TSA [34], our results suggest that 5 μM LmPTR1 is required to achieve a good signal:noise ratio (12 x) (Fig. 2).

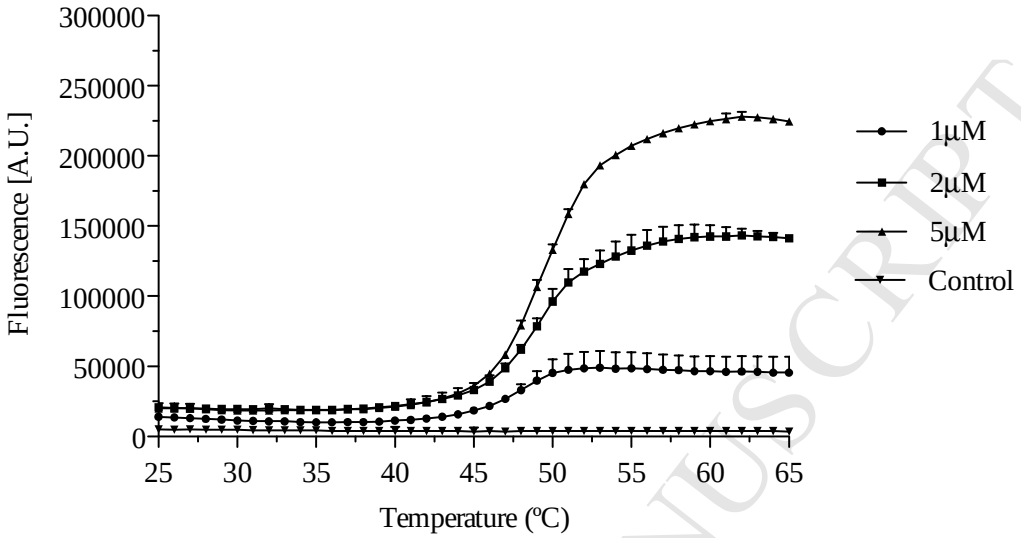

Fig. 2. Unfolding transition of LmPTR1 in 20 mM Sodium acetate pH 4.7 buffer

Our studies also suggest that LmPTR1 is stable either in pH 4.5 or pH 7.5, once Tm values does not vary significantly ($p > 0.05$) between these conditions (Fig. 3). This result makes it possible to assay putative LmPTR1 inhibitors in physiological conditions, whereas traditional kinetic assay requires pH 4.7. For a matter of comparison though, TSA screening and kinetic assays were carried out under the same conditions (pH 4.7).

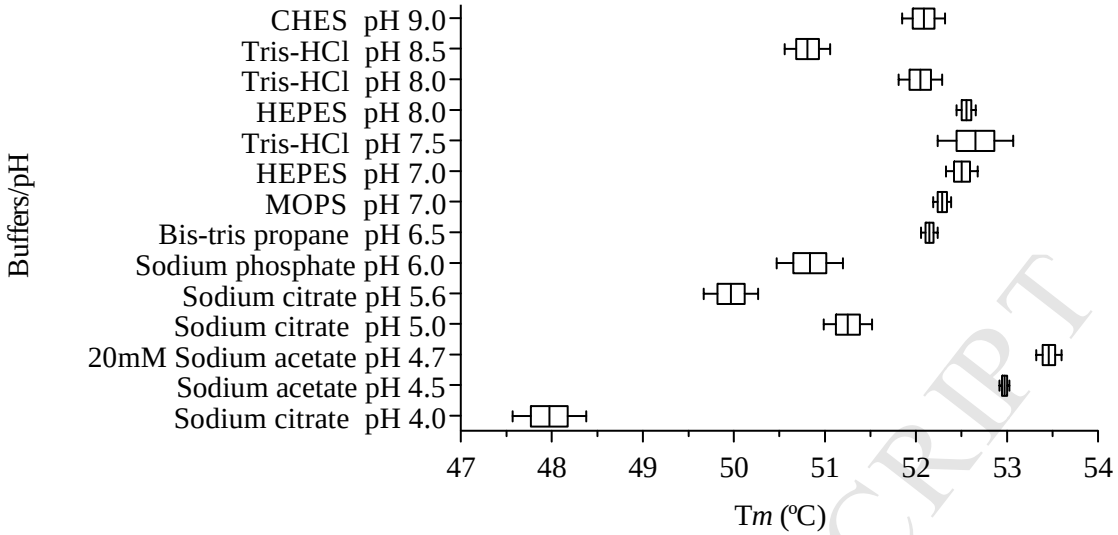

Fig. 3. Midpoint temperatures of the LmPTR1-unfolding transition (Tm) in different pHs. LmPTR1 (5 μM) and buffer concentration (50 mM) were kept constant.

Finally, TSA suggests that DMSO does not significantly affect (p> 0.05) LmPTR1 Tm below 20 % (Fig. 4). However, 5 % was enough to carry out the assay with **2a-g**.

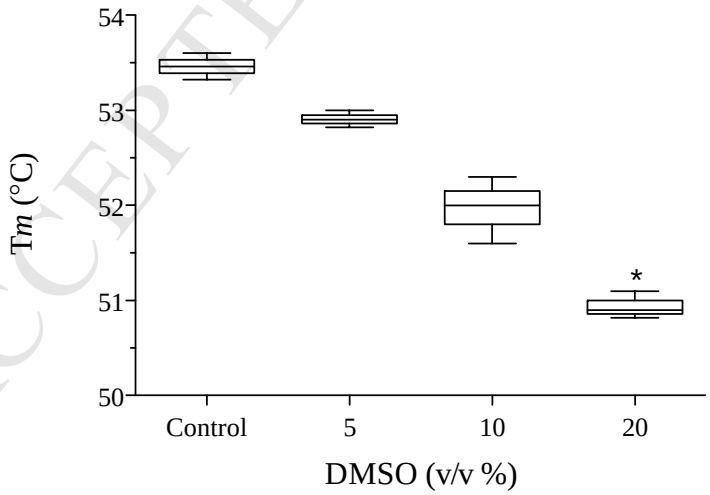

Fig. 4. Midpoint temperatures of the LmPTR1-unfolding transition (Tm) in the presence of three DMSO concentrations. (Kruskal-Wallis ANOVA, n=3). * = $p < 0.05$.

2.2.2 Screening and IC50 determination

In HTS campaigns, compounds with positive ΔTm> 1.0 ^{o}C are considered as primary hits for secondary assay [35]. In case a similar strategy was taken, **2f** would be discarded (Fig. 5) and all other 6 compounds would be considered as hits. However, this arbitrary set point lacks statistical significance and making assumptions on single dose assays can be quite misleading. In order to circumvent such problems further studies were carried out with compounds which significantly shifted ($p < 0.05$) LmPTR1 Tm (**2e** and **2d)**.

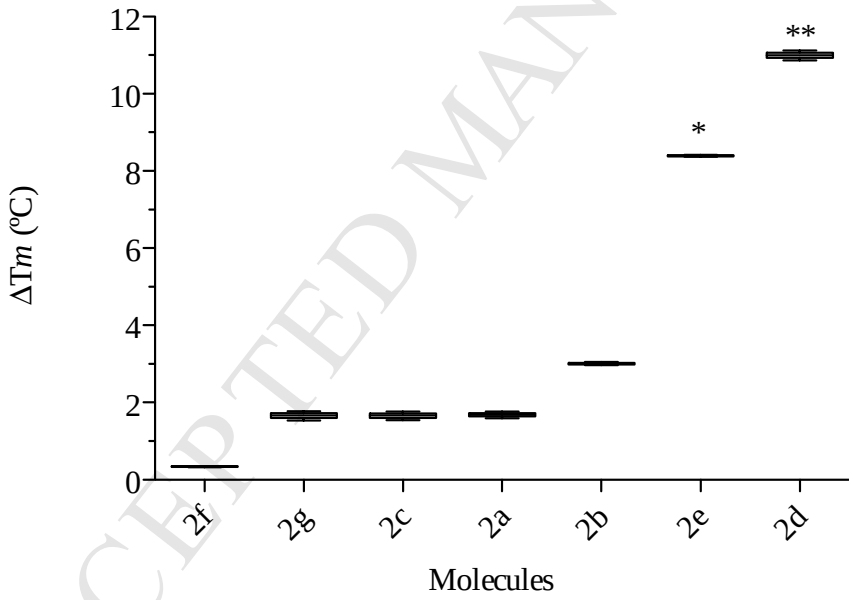

Fig. 5. Displacement of LmPTR1 Tm values (control= 48.45 ℃) d ue to thiazolidine-2,4-dione derivatives (50 μM) (Kruskal-Wallis ANOVA, n=3). ** = $p < 0.01$ * = $p < 0.05$.

Both compounds show a dose-response effect over the thermal stability of LmPTR1 that reaches a maximum above 200 μM (Fig. 6 A and 6 B). However, Tm conversion to accurate Ki values requires knowledge of the unfolding enthalpy (ΔUH), which cannot be directly measured through TSA [36].

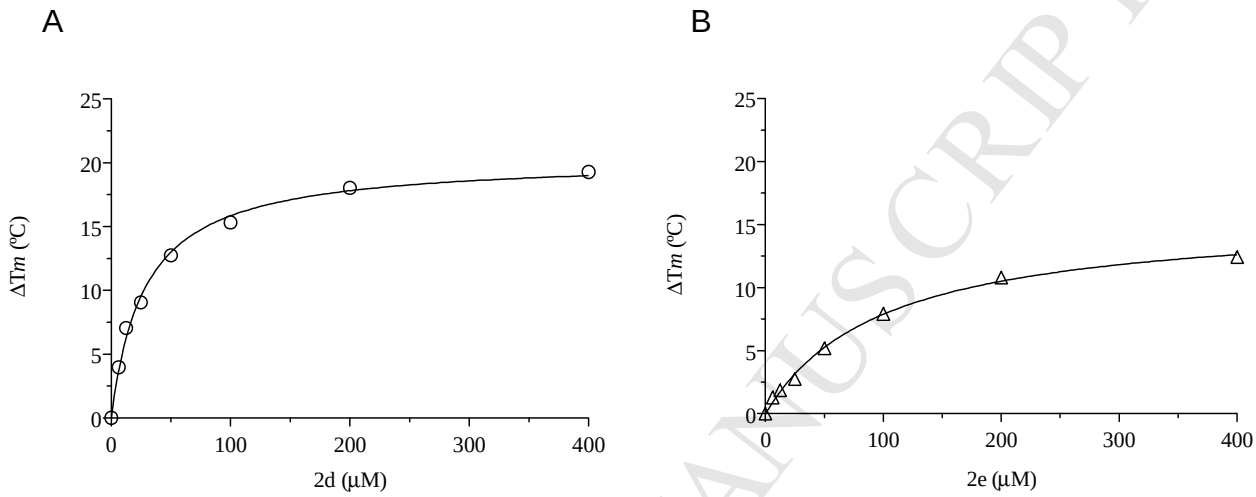

Fig. 6. Dose-response effect of **2d** (A) and **2e** (B) over LmPTR1 thermal stability.

Alternatively, we resorted to classical kinetic assays [37] to measure the compounds relative potency and, for a matter of comparison, all thiazolidine-2,4-dione derivatives (2a-g) were assayed again (Fig. 7).

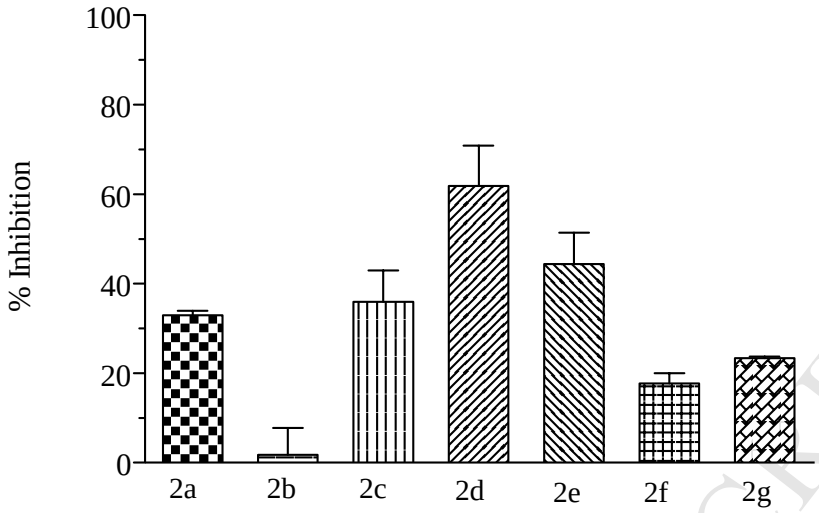

Fig. 7. Effect of thiazolidine-2,4-dione derivatives (50 µM) over the catalytic activity of LmPTR1.

The inhibitory profile of compounds **2a-g** over the catalytic activity of LmPTR1 does not agree with the temperature shifts seen in TSA. Although, **2d** and **2e** appear as the two most promising compounds again, the ranking of the other compounds is quite different. For instance, if thermal shift alone was considered as a selection criteria, **2b** would be the third best hit (ΔTm= 3.01 ± 0.03 ℃). However, single-concentration assay shows that it does not inhibit LmPTR1 (both assays were carried out under identical pH). **2c** on the other hand (ΔTm= 1.7 ± 0.08 ℃) comes from the fifth to the third best position (36 % ± 6.0 inhibition at 50 µM). This apparent contradiction might be related to the fact that standard TSA does not take into account the ES to ES* transition. Aiming to further investigate this matter, the IC50 values of these three inhibitors were determined (Fig. 8).

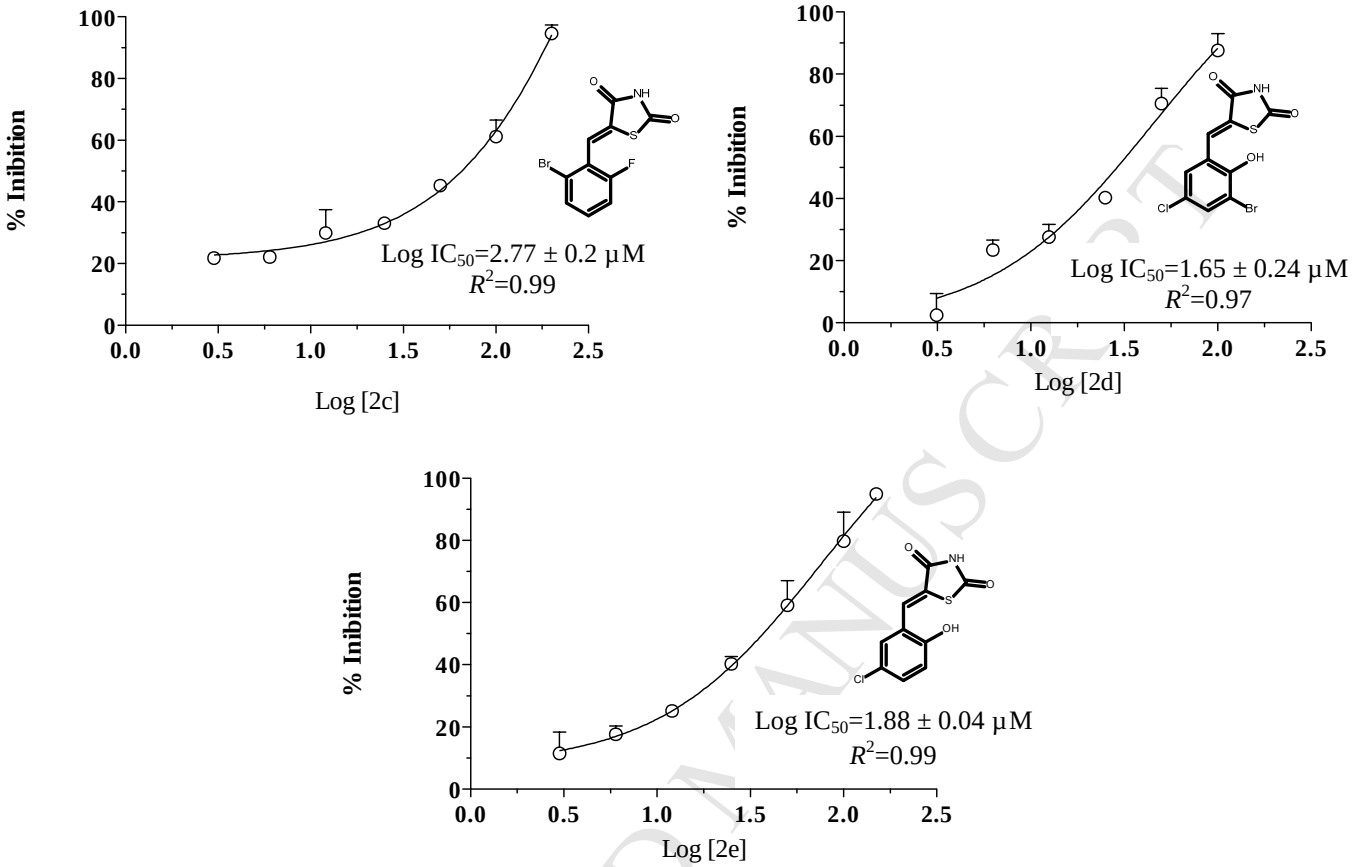

Fig. 8. Dose-response curve for three most promising thiazolidine-2,4-dione derivatives in single dose-assay. IC50 values were calculated by non-linear regression using 3-parameters equation and standardized response, as available in GraphPad Prism® 5.0 software.

The results confirm that **2d** (IC50 44.67 ± 1.74 □M) and **2e** (IC50 75.86 ± 1.10 □M) are micromolar inhibitors of LmPTR1, whereas **2c** (IC50 588.84 ± 1.58 □M) should be considered a low milimolar inhibitor. Taking these results into consideration, only **2d** and **2e** were considered as promising compounds for further studies. The lower potency of compound 2c might be related to lack of

complementarity towards its binding site (no substituent in *meta* or *para* positions) or the distorted orientation of the phenyl ring regarding the thiazolidine-2,4-dione ring (two *orto* substituents). Molecular dynamics studies (section 3) hints that the second hypothesis should be discarded, but further studies are required to clarify this matter.

2.2.3 Inhibition mechanism studies

It has been shown that the inhibition mechanism (competitive, noncompetitive, uncompetitive) can be determined by TSA [38]. As **2d** and **2e** have high structural similarity, it is reasonable to assume they have the same inhibition mechanism. Thus, the most potent compound was chosen as a representative compound for the role series and its effect over the thermal stability of LmPTR1 in the presence of either Biopterin (substrate) or NADPH (cofactor) was evaluated (Fig. 9).

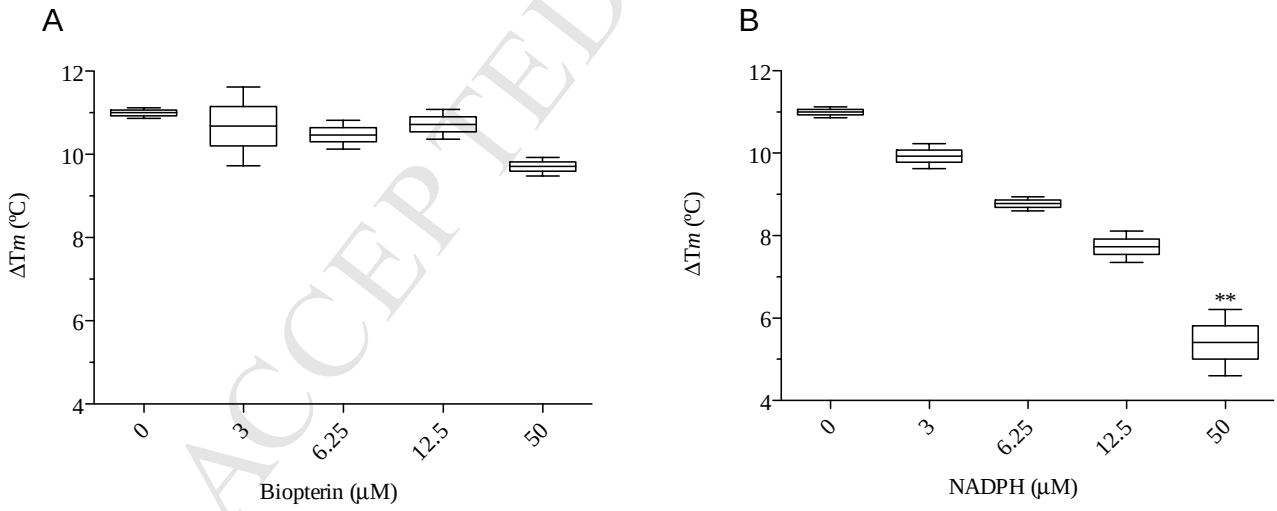

Fig. 9. Effect of Biopterin (A) or NADPH (B) over the thermal shift due to **2d** (50 μM) (Kruskal-Wallis ANOVA, n=3). * = $p \leq 0.01$.

As increasing concentrations of NADPH are added to the assay, thermal shift stabilization due to **2d** begins to decrease and this effect becomes statistically significant ($p = 0.01$) at NADPH 50 μM. On the other hand, increasing concentrations of Biopterin do not significantly change the thermal shift due to **2d**. Together, these results suggest that **2d** is a noncompetitive inhibitor that binds in the same site as the cofactor. In order to confirm this hypothesis, the effect of **2d** over LmPTR1 KM and VMAX was investigated.

A noncompetitive inhibitor would not affect LmPTR1 affinity towards biopterin (formation of the (E-S) complex) as measured by the apparent value of KM, but change the subsequent chemical steps (ES to ES* transition) that influence VMAX [39]. This simplistic approach is valid for LmPTR1 (ping-pong mechanism [40]) as long as a saturating concentration of cofactor (40 μM) is employed. Accordingly, a double-reciprocal plot of the velocity as a function of biopterin (substrate) at varying concentrations of the **2d** (Fig. 10 A) shows a set of lines that intercept the x-axis at the same point (-1/KM), whereas they cross the y-axis (1/VMAX) at different values.

This behavior is compatible with a noncompetitive inhibitor, which might bind in the NADPH (cofactor) binding site or elsewhere (allosteric inhibitor). In order to further investigate this matter, we repeated the kinetic assay keeping the substrate at saturating concentration (40 μM) and varying the cofactor concentration. This time, the double-reciprocal plot of the velocity as a function of NADPH (cofactor) at varying concentrations of the **2d** (Fig. 10 B) shows that the VMAX values remained unchanged at all inhibitor concentrations (set of lines that intercept the y-axis, 1/VMAX), whereas the apparent values of KM (the x-intercept lines, -1/KM) increased with increasing inhibitor concentration by a factor of $(1 + [I]/Ki)$. Thus, it is clear that **2d** competes with NADPH towards LmPTR1.

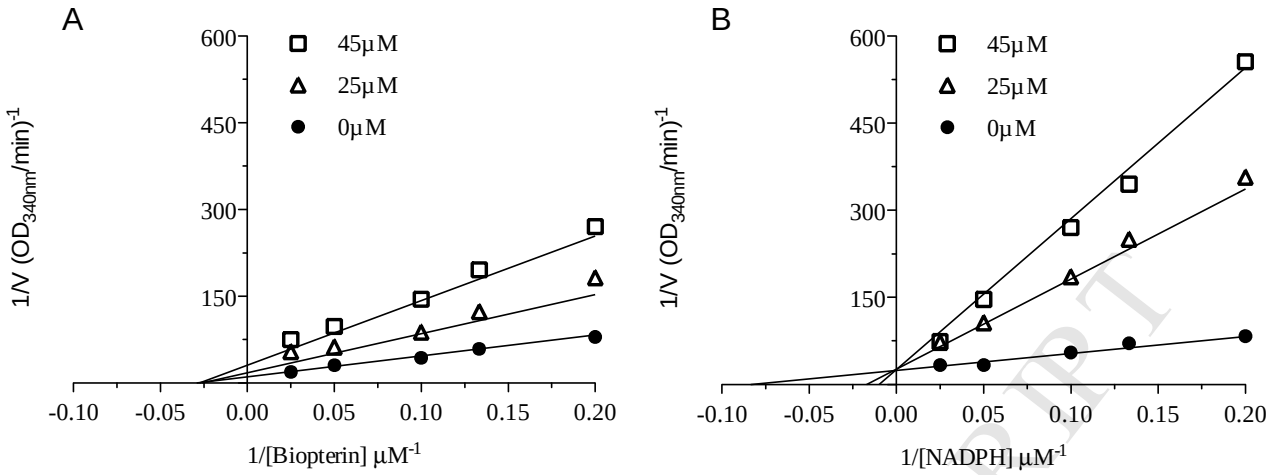

Fig. 10. Inhibition profile of **2d** against LmPTR1. Kinetic experiments were conducted in the presence of increasing concentrations of the inhibitor: ● = 0 µM; Δ= 25 µM; □= 45 µM. Panel A: [Biopterin]= 40 µM. Panel B: [NADPH]= 40 µM.

3 Molecular modeling studies

Although previous studies are crucial to understand **2d** inhibition mechanism and potency, they do not provide a molecular insight that would guide the design of second-generation thiazolidine-2,4-dione inhibitors. In order to accomplish this goal, molecular modeling approaches, such as docking and molecular dynamics were employed. Accordingly, **2d** interaction profile toward LmPTR1 was probed with Surflex-Dock [41], which relies on an idealized representation of the ligand within the active site (protomol) to describe the search space. As our previous data support **2d** binding to the NADPH site. Then, the protomol was automatically calculated using the crystallographic coordinates of this cofactor (PDB: 1E92). Redocking (data not shown) was carried out to guarantee that default search and scoring parameters were enough to find poses with RMSD< 2 Å from the crystallographic conformation. Once the top scoring pose for NADPH has a RMSD= 0.70 Å, only the best ranking

pose of **2d** was considered further. **2d** putative binding profile is similar to the one seen for the adenine ring of NADPH, within LmPTR1 cofactor site: The thiazolidine-2,4-dione ring is positioned within adequate range to pi-pi stack with His^{38}, whereas carbonyl and NH moieties hydrogen bond to Ser^{111} (2.90 Å), Leu^{66} (3.00 Å), and Asp^{142} (2.60) (Fig. 11 A). Postigo and coworkers [17] have found a similar binding profile for 4-thioxo-thiazolidine-2-one derivatives within *Schistosoma mansoni* purine nucleoside phosphorylase cofactor binding site. Thus, our results support the hypothesis that thiazolidine-2,4-dione ring acts as bioisosteric replacement for the adenine or xanthine ring, depending on its substituents.

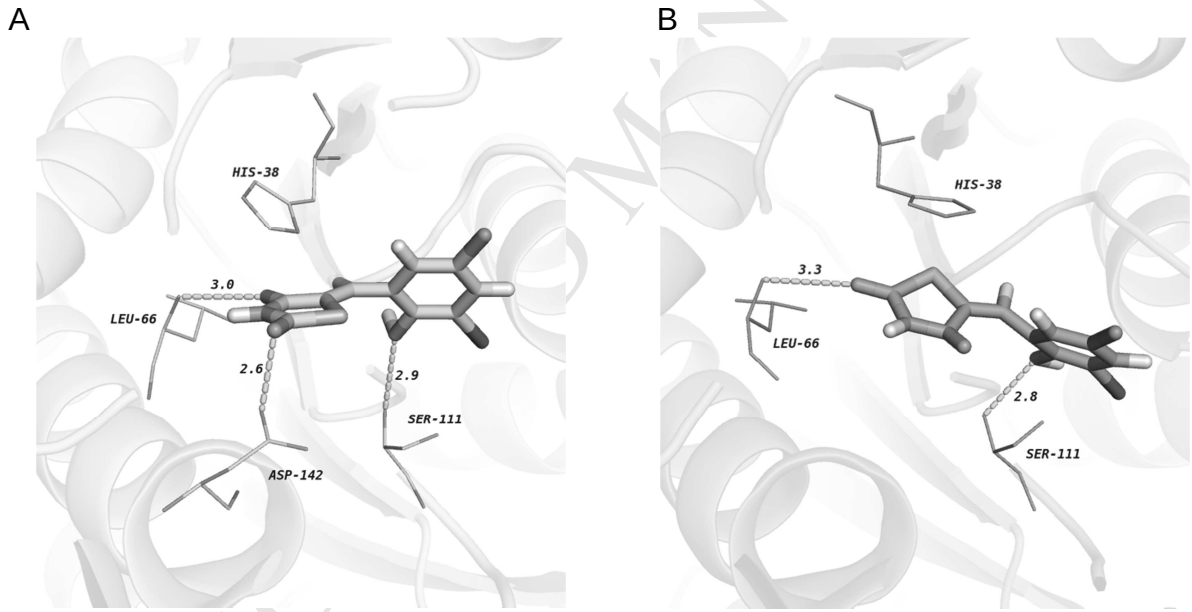

Fig. 11. Putative binding profile of **2d** towards LmPTR1 NADPH binding site. (A) best ranked pose according to Surflex-Dock. (B) representative conformation of 2D according to MD simulations (50000 ps). The NADPH binding site residues are depicted in line, whereas **2d** is depicted in stick model. The hydrogen bonds are displayed as dashed line and distances are measured in angstroms. The figure was generated using the PyMOL 1.3 software.

Although docking results are compatible with kinetic and TSA experimental data, induced fit flexibility cannot be taken into account as the protein residues heavy-atoms were considered as rigid, during the docking protocol. Hence, **2d** interaction profile within the NADPH binding might not be accurately described by docking studies. In order to overcome this dilemma, molecular dynamics simulations were carried out with GROMACS 4.5.6 software [42]. Overlay of LmPTR1 crystallographic structures suggest that main chain flexibility due to ligand binding is rather small. Hence, side-chain flexibility only was investigated in our DM studies.

In order to guarantee that our system (PTR1:**2d**) is stable throughout the MD simulations (50000 ps) its main-chain root mean square deviation (RMSD) was compared to the APO structure built from crystallographic coordinates of 1E92 (Fig. 12). Taking into account the last 20000 picoseconds of the simulation, when both structures are stable, PTR1:2d complex shows a lower RMSD value than the APO structure (0.45 *vs.* 0.61 nm). This result is expected and in good agreement with TSA assays described herein.

This preliminary encouraging result led us to focus on the interaction profile of **2d** during a simulation length long enough to allow rearrangement of side chains, according to Pikkemaat et al., [43]. In order to do so, a representative structure from the productive phase (30000-50000 ps) was selected (Fig. 11 B), according to RMSD criteria [44].

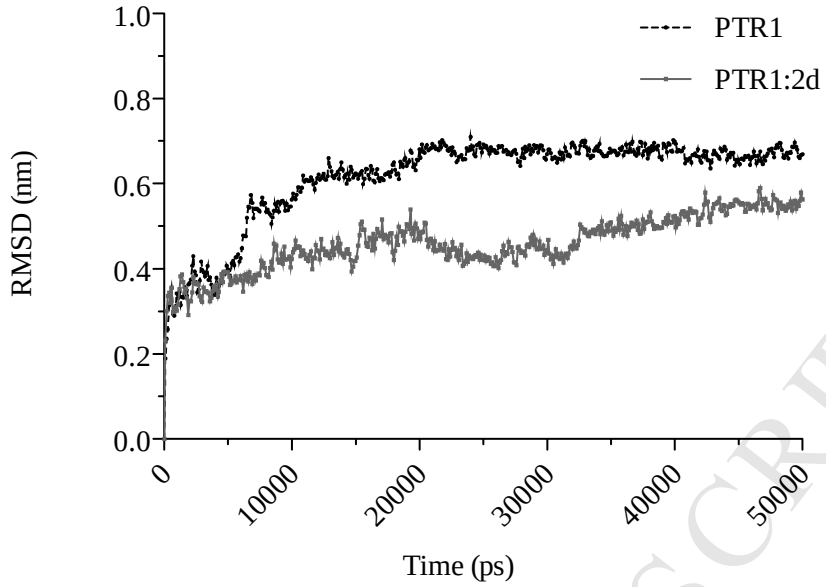

Fig. 12. Root-mean-square deviation calculated on Cα positions over trajectory with respect to their initial structures.

Visual analysis of **2d** interaction profile, following DM simulation, shows that: A) Thiazolidine-2,4-dione and phenyl ring are not parallel to each other, thus suggesting that steric hindrance of *orto* substituents does not prevent the inhibitors to adopt the bioactive conformation; B) His^{38} is parallel to **2d** thiazolidine-2,4-dione ring, thus the pi-pi stacking suggested by docking is supported by subsequent studies. A similar trend is seen for the hydrogen bonds to Ser^{111} and Leu^{66}. However, H-bonding to Asp^{142} is not present in the representative structure. In order to exclude the bias from a single structure analysis, **2d** interaction profile was analyzed along the productive phase (interaction stability trough time). This analysis confirms that H-bonding to Ser^{111} and Leu^{66} hold for 28 % and 87 % of the simulation, respectively.

3. Conclusions

The structure-guided approach employed in this work proved effective to identify a novel series on LmPTR1 inhibitors whose scaffold is completely different from the molecules previously reported by Cavazzuti et al.,[14] and Ferrari et.al.,[15]. Moreover, the most potent thiazolidine-2,4-dione derivative (**2d**) is the first non-competitive inhibitor of LmPTR1 described. The two-digit micromolar potency (IC50= 44.67 μM) presented by **2d** shall be rapidly improved by drug design efforts guided by the putative binding profile described in this work. The synergic use of experimental results (kinetic and TSA assays) proved invaluable to correctly explore the full potential of docking and DM and help to clarify the binding profile of this new lead within LmPTR1 NADPH binding site. In conclusion, the results reported herein lay the basis for the development of a new class of non-competitive LmPTR1 inhibitors.

4. Experimental section

4.1 Chemistry

4.1.1 Experimental

All melting points were measured in a capillary tube on a Buchi apparatus. Infrared spectra (1 % KBr, cm^{-1}) pellets were recorded on a Bruker IFS66 spectrophotometer and are uncorrected. The ^{1}H NMR and ^{13}C NMR spectra were recorded on a VARIAN VNMRS 400-MR, using 400 MHz for ^{1}H and 75.4 MHz in DMSO-d_6 using tetramethylsilane (TMS) as the internal standard. Chemical shift values are reported in parts per million units. The ^{13}C NMR in $CDCl_3$ and DMSO was maintained at 25 ºC using Me_4Si (TMS) as an internal standard. The following abbreviations were used to

indicate the peak multiplicity: s (singlet), d (doublet), dd (double doublet), ddd (double doublet, doublet), t (triplet), and m (multiplet). The chemical shifts were reported in δ units and the coupling constants (J) were reported in Hertz. Mass spectra were recorded on a Varian MAT 711 spectrometer 70 eV electron impact. Thin layer chromatography (TLC) was performed on pre-coated silica plates (Merck Kiesegel 60 F_{254}) and the spots were visualized under ultraviolet light ((254 nm) / long (365 nm) UV wavelength). The chemical reagents were supplied by Sigma-Aldrich (USA) and were used without further purification. Purity of the compounds was confirmed by TLC (Kiesel gel 60 G F 254) using the appropriated system for each compound.

4.1.2 Procedure for preparation - synthesis of thiazolidine-2,4-dione (1)

The thiazolidine-2,4-dione (1) was obtained by the method described by Libermann in 1948 and modified by Albuquerque 1995 [29,45,46]. This reaction occurs by condensation of monochloroacetic acid and thiourea in an aqueous medium under reflux for 24 hours [30,31].

Molecular formula $C_3H_3O_2NS$; yield 78 %; mp 118-120 ºC; Rf 0.48 (0.9:0.1 $CHCl_3$/MeOH). Recrystallization: water.

MF $C_3H_3NO_2S$, MW 117.1264, Rdt 85 %, Rf 0.46 (0.9: 0.1 $CHCl_3$/MeOH) MP 120-122 ºC.

4.1.3 General method for the synthesis of 5-arylidene-thiazolidine-2,4-diones (2a-g)

The compounds (**2a-g)** were synthesized according to protocol described in [26,27,43]. Briefly, a solution of thiazolidine-2,4-dione (0.200 g, 1.70 x 10^{-3} mol) in ethanol, (7.0 mL) containing piperidine (2 drops) and aromatic aldehyde (0.184 g,

2.25 x 10^{-3} mol) was heated (70 ºC), under stirring, for 5 to 9 hours. The reaction progress was monitored by thin layer chromatography (TLC). After this period, the product was cooled in an ice bath, filtered and recrystallized with an appropriate solvent. The resulting precipitate was filtered off and recrystallized from acetic acid to give the compounds (**2a-g**). The yields obtained were considered satisfactory.

4.1.3.1 (Z)-5-(2,4-dichlorobenzylidene-thiazolidine-2,4-dione (2a):

MF $C_{10}H_5Cl_2NO_2S$, MW 274.1232, Yield. 85 (%), Rf 0.51 (9.8: 0.2 $CHCl_3$/MeOH), MP 203 ºC Recrystallization: ethanol; IR, (KBr, cm^{-1}): 3054 (N-H), 1712 (C=O), 1433 (C=C). ^{1}H RMN (400 MHz, DMSO-d_6, δ ppm): 7.81 (s, 1H, C=CH), 12.64 (s broad, 1H, N-H). 7.23 (s, $1H_{(3)}$ Ar), 7.26 (d, $1H_{(5)}$, Ar J=7.52 Hz), 7.36 (d, $1H_{(6)}$, Ar, J=7.51 Hz). ^{13}C RMN and DEPT (75.5 MHz, DMSO-d_6; δ ppm): 119.18, 135.58, 128.31, 137.12, 127.91, 128.97, 142.12 CH=C, 125.31 (heterocycle), 167.20 ($C=O_{(2)}$, 166.19 $C=O_{(4)}$. $HRMS^+$, calculated: 274.1233, found: 274.1073**.**

4.1.3.2 5-(3,4-dichlorobenzylidene-thiazolidine-2,4-dione (2b):

MF $C_{10}H_5Cl_2NO_2S$, MW 274.1232, Yield. 73 (%), Rf 0.50 (9.5: 0.5 $CHCl_3$/MeOH), MP 174 ºC. Recrystallization: ethanol; IR, (KBr, cm^{-1}): 3056 (N-H), 1712 (C=O), 1433 (C=C). ^{1}H RMN (400 MHz, DMSO-d_6, δ ppm): 7.26 (s, $1H_{(2)}$, Ar), 7.18 (d, $1H_{(5)}$, Ar J=7.355 Hz), 7.14 (d, $1H_{(6)}$, Ar, J=7.14 Hz), 7.76 (s, 1H, CH=C), 11.98 (s broad, 1H, NH). ^{13}C RMN and DEPT (75.5 MHz, DMSO-d_6; δ ppm): (134.21, 133.75, 129.11, 131.15, 130.11, 127.12 Ar); (117.79, heterocycle) 146.15 CH=C); 169.12 ($C=O_{(2)}$, 167.23 $C=O_{(4)}$. $HRMS^+$, calculated: 274.1234, found: 274.1215.

4.1.3.3 (Z)-5-(2-Bromo-6-fluorobenzylidene)-thiazolidine-2,4-dione (2c):

MF $C_{10}H_5BrFNO_2S$, MW 302.1196, Yield. 78 (%), Rf 0.40 (9.8: 0.2 $CHCl_3$/MeOH), MP 115-116 ºC, IR, (KBr, cm^{-1}): 3164 (N-H), 1703 (C=O_4), 1445 (C=O_2), 1322 (C=C). ^{1}H RMN (400 MHz, DMSO-d_6): δ 7.09-7.15 (t, 1H$_{(3)}$, Ar, J=9 Hz); 7.23-7.30 (m, 1H$_{(4)}$, Ar); 7.46 (d, 1H$_{(5)}$, Ar, J=7.8 Hz); 7.64 (s, 1H$_{(5)}$, C=CH); 11.71 (s broad, 1H, NH). ^{13}C RMN and DEPT (75.5 MHz, DMSO-d_6): δ 115.58, 127.28, 127.32, 128.94, 129.98, 131.88, (115.80 heterocycle); CH=C 142.29; 167.19 (C=O_2); 166.19 (C=O_4.). HRMS$^+$: Calculated: 302.1678; found: 302.1096.

4.1.3.4 (Z)-5-(2-Hydroxy-3-bromo-5-chlorobenzylidene)-thiazolidine-2,4-dione (2d):

MF $C_{10}H_5BrClNO_3S$, MW 334.5736, Yield 73 %, Rf 0.47 (9.6:0.4 $CHCl_3$/MeOH), MP 197 ºC; IR, (KBr, cm^{-1}): 3157 (N-H), 1698 (C=O_4), 1592 (C=O_2), 1449 (C=C). ^{1}H NMR (400 MHz, DMSO-d_6): δ, 7.07 (s, 1H$_{(4)}$, Ar), 7.35 (s, 1H$_{(5)}$, Ar); 5.18 (s, 1H, OH), 8.05 (s, 1H, C=CH). 11.98 (s 1H, NH). ^{13}C NMR and DEPT (DMSO-d_6, 75.4 MHz, δppm): (δ 119.83, 134.57, 122.85, 130.40, 123.59, 136.57 Ar), 123.40 heterocycle, 143.79 (C=CH) 168.32 (C=O_2), 166.47 (C=O_4). HRMS$^+$, calculated: 334.5736; found: 335.2612.

4.1.3.5 (Z)-5-(2-Hydroxy-5-chlorobenzylidene)-thiazolidine-2,4-dione (2e):

MF $C_{10}H_6ClNO_3S$, MW 255.6775, Yield 79 %, Rf 0.45 (0.9:0.1 $CHCl_3$/MeOH) MP 207 ºC. IR, (KBr, cm^{-1}): 3128 (N-H), 1723 (C=O_4), 1645 (C=O_2), 1588 (C=C). ^{1}H RMN (400 MHz, DMSO-d_6): δ 7.07 (d, 1H$_{(3)}$, Ar, J=7.7 Hz), 7.38 (dd, 1H$_{(4)}$, Ar, J=7.5 Hz, J=1.5 Hz), 7.34 (s, 1H$_{(6)}$, Ar), 7.98 (s, 1H, C=CH), 5.15 (s 1H, OH), 10.86 (s, 1H, NH). ^{13}C NMR and DEPT (75.5 MHz, DMSO-d_6): δ (119.74, 121.67, 123.09, 123.86,

125.57, 127.37 Ar); 118.59 heterocycle, 147.02 (C=CH), 167.43 ($C=O_2$), 165.8 ($C=O_4$). $HRMS^+$, calculated: 255.6725; found: 254.092.

4.1.3.6 (Z) 5-(3,4-dichlorobenzylidene-thiazolidine-2,4-dione (2f):

MF $C_{10}H_5Cl_2NO_2S$, MW 274.1232, Yield. 77 (%), Rf 0.40 (9.8:0.2 $CHCl_3$/MeOH), MP 115-116 ºC; Recrystallization: ethanol; IR, (KBr, cm^{-1}): 3058 (N-H), 1715 (C=O), 1625 (C=O), 1432 (CH=C). ^1H RMN (400 MHz, DMSO-d_6, δ ppm): 7.19 (d, $H_{(3,5)}$, Ar J=7.38 Hz); 7.21 (t, $1H_{(4)}$, Ar J=7.68 Hz, J= 1.51 Hz), 7.71 (s, 1H, CH=C), 11.97 (s broad, 1H, NH). ^{13}C RMN and DEPT (75.5 MHz, DMSO-d_6, δ ppm): (120.22, 137.18, 128.13, 140.20, 128.13, 128.11 Ar), 118.81 heterocycle, 140.35 CH=C, 1168.35 ($C=O_{(2)}$), 167.25 ($C=O_{(4)}$). $HRMS^+$, calculated: 274.1211 found: 274.1121.

4.1.3.7 (Z)-5-(2-Bromo-5-methoxybenzylidene)-thiazolidine-2,4-dione (2g):

MF $C_{11}H_8BrNO_3S$, MW 314.1551, yield 79 %, Rf 0.5 (9.6:0.4, $CHCl_3$/MeOH), MP 212-213 ºC; IR, (KBr, cm^{-1}): 3125 (N-H), 1702 ($C=O_4$), 1603 ($C=O_2$), 1471 (HC=C). ^1H MNR (400 MHz, DMSO-d_6 δ ppm): 3.81 (s, 3H, OCH_3), 7.31 (d, $1H_{(3)}$, Ar, J=7.3 Hz), 7.17 (dd, $1H_{(4)}$, Ar, J=7.5 Hz, J=1.3 Hz), (s $1H_{(5)}$. Ar); 7.78 (s, 1H, C=CH), 12.76 (s broad, 1H, N-H). ^{13}C NMR and DEPT (75.5 MHz, DMSO-d_6): δ 55.63 (OCH_3); 134.03, 114.01, 134.91, 127.61, 117.36, 159.39 (Ar); 142.28 (C=CH); 166.12, ($C=O_{(2)}$, 165.49 ($C=O_{(4)}$. $HRMS^+$, calculated: 314.1551; found: 314.1081.

4.2 In vitro assays

4.2.1 Protein production

A pet15-b construct encoding LmPTR1 was kindly provided by Prof. Willian Hunter [14]. This plasmid codes for a hexa-histidine tag on the N-terminus of the gene product and allows the use of affinity chromatography to purify the enzyme.

The *E. coli* strain BL21(DE3) was heat-shock transformed with pET-LmPTR1 and selected on Luria-Bertani (LB) agar plates containing 50 μg mL^{-1} of ampicillin. Bacteria were cultured in LB broth with 50 μg mL^{-1} of ampicillin to mid log phase at which point expression was induced with 0.5 mM isopropyl-β-D-thiogalactopyranoside (IPTG) and cell growth continued with vigorous agitation for 16h at 18 ºC. Cells were harvested by centrifugation (2800g) at 4 ºC and then resuspended in 50 mM Tris-HCl pH 7.5, 250 mM NaCl. The cells were disrupted by sonication (10 x 15 s bursts with 30 s intervals between each burst) on an ice-bath. After the insoluble debris were separated by centrifugation (16 000 g for 30 minutes at 4 ºC), the clear supernatant, containing LmPTR1, was loaded on a 1 mL column Ni-NTA agarose affinity resin (Qiagen) equilibrated with 50 mmol L^{-1} Tris-HCl, pH 7.5, buffer containing 250 mmol L^{-1} NaCl and 20 mmol L^{-1} imidazole. Then, the column was washed with 20 column volumes of 50 mmol L^{-1} Tris-HCl, pH 7.5, buffer containing 250 mmol L^{-1} NaCl and100 mmol L^{-1} imidazole. Next, the target protein was eluted with followed 20 column volumes of 50 mmol L^{-1} Tris-HCl, pH 7.5, buffer containing 250 mmol L^{-1} NaCl and 400 mmol L^{-1} imidazole.

4.2.2 Thermal shift assays (TSA)

4.2.2.1 TSA optimization

Thermal shift assays were carried out with a using an Applied Biosystems 7500 RT-PCR (Applied Biosystems, Foster City, CA USA) fitted with custom filter sets. The data was recorded in Applied Biosystems 7500 Software v2.0. Initially, conditions of the assay (choice of buffer, protein concentration and DMSO concentration) were optimized for LmPTR1. Each parameter was tested in triplicate on a 96-well PCR plate (PCR plates 96 well BioRad®), manually sealed with transparent capping strips (Flatcap strips BioRad®). The final protein concentration in optimization trials was 5 µM, except for the determination of optimum PTR1 concentration, which varied from 1 to 5 µM. Fluorescence changes were monitored with SYPRO Orange® dye, using 492 and 610 nm wavelengths for excitation and emission respectively

4.2.2.2 TSA screening

Each of the seven thiazolidine-2,4-dione derivatives (**2a-g**) was screened at 50 µM in triplicate. 1µL of each compound (1mM DMSO stock solution) was added to 19 µL *Lm*PTR1 in 50 mM Sodium acetate pH 4.7 (final concentration 5 µM) containing 1 µL of 1:100 diluted SYPRO Orange dye®. Each compound was assayed in triplicate and Tm values were compared to reference wells that were identical to the experiment wells except that DMSO was used in place of the compound solution. The assays were carried out in 96-well PCR plate (PCR plates 96 well BioRad®), sealed with transparent capping strips (Flatcap strips BioRad®) as described previously. Thermal shift assays was carried out from 25 to 85 ºC in

increments of 1 ˚C per minute. Fluorescence data (Raw data) was recorded using the Applied Biosystems 7500 Software v2.0, and then exported to Excel 2007 worksheet (ftp://ftp.sgc.ox.ac.uk/pub/biophysics) [20] for processing and analysis. Tm values employed for compounds comparison were those calculated from the non-linear fitted melting curves (Boltzmann sigmoidal function) implemented in GraphPad Prism version 5.0 for Windows (GraphPad® Software, San Diego, CA, USA, www.graphpad.com).

4.2.2.3 TSA characterization of thiazolidine-2,4-dione *LmPTR1 inhibitors*

The type of inhibition (competitive, non-competitive, uncompetitive) was investigated by repeating the TSA screening assay in the presence of varying concentrations of cofactor (NADPH= 0.0, 3.0, 6.25, 12.5, 50 μM) or substrate (Biopterin= 0.0, 3.0, 6.25, 12.5, 50 μM). All measurements were carried out in triplicate and ΔTm values were compared by non-parametric ANOVA Kruskal-wallis.

4.2.3 Kinetic measurements

Kinetic measurements were carried out spectrophotometrically with the aid of a Schimadzu UV-1800 UV–Vis spectrophotometer, using a standard assay described by Dawson and coworkers [47]. Briefly, 10 μL of NADPH (2 mM in 0.02 M NaOH) solution was added to *Lm*PTR1 (0.2 μM), 10 μL of biopterin (2 mM in 0.1M NaOH) and 50 μL (0-1 mM in 5% DMSO (v/v)) of compound in 20 mM sodium citrate (pH 4.7) (total volume 930 μl). A decrease in absorbance was followed spectrophotometrically at 340 nm during 60 s. All measurements were carried out in

triplicate at 30 ^{o}C and IC50 values were calculated by non-linear regression, using measurements from at least six inhibitor concentrations, as available in Sigma Plot V.12.0.

4.2.3.1 Kinetics characterization of thiazolidine-2,4-dione *LmPTR1 inhibitors*

The type of inhibition was determined under the same reaction conditions described in 4.2.3 but using two fixed inhibitors concentrations and varying either the substrate or the cofactor concentrations (BPT=5.0, 7.5, 10.0, 20.0 and 40.0 μM/ NADPH= 5.0, 7.5, 10.0, 20.0 and 40.0 μM). The reported values represent means of at least three individual experiments.

4.3 Molecular modeling studies

4.3.1 Docking studies

Molecular docking and scoring protocols, as implemented in Surflex-Dock [41], were employed to search for reasonable binding poses of the ligands within the NADPH binding pocket of *Lm*PTR1. The structures of thiazolidine-2,4-dione inhibitors were sketched in ChemDrawBio 12.0 and then converted to 3D using SYBYL®-X 2.0 “translate molecular files” default options. Next, all 3D structures were energetically minimized through Conjugated-gradient protocol (convergence criterion=0.001 Kcal/mol; maximum iteration = 50000), using Tripos force field, Gasteiger-Huckel charges and an implicit solvent environment (Dielectric constant= 80.0). This strategy aimed at avoiding possible bond length or bond angles distortions present in any molecule. The X-ray crystallographic structure of *Lm*PTR1

in complex with dihydrobiopterin and NADP+ at 2.20 Å resolution (PDB ID 1E92), used in the docking protocols, was retrieved from the PDB databank and all its ligands and water molecules were discarded. Next, hydrogen atoms were added in standard geometry orientations using the Biopolymer module implemented in SYBYL®-X 2.0. Within this module, Histidines, glutamines, and asparagines residues within the binding site were manually checked for possible flipped orientation, protonation, and tautomeric states. As the kinetic assays were carried out in pH 4.7, Histidine residues were considered as fully protonated in all docking runs, whereas ASP-181 and ASP-251 was kept deprotonated. The search space was centered on NADPH crystallographic coordinates and its limits defined using default protomol generation parameters (bloat=0.0, Threshold=0.5). Poses obtained by Surflex-Dock search parameters were visually inspected within PyMOL™ 1.3 software [48]. Only poses that are consistent with kinetic studies were considered further.

4.3.2 Molecular Dynamics

The Gromacs 4.6.5 package [42] was used to prepare the protein. The ligand topology was constructed in the Automated Topology Builder (ATB) server (http://compbio.biosci.uq.edu.au/atb/) for the Molecular Dynamics (MD) simulations. The initial coordinates of PTR1:2d complex were generated with Surflex-Dock [41] and simulated in electrically neutral condition by adding appropriate number of sodium counterions. The system was solvated in an octahedron box of SPC/E water model with a 1.4 nm distance between the protein surface and the box boundary. Linear constraint algorithm was employed to restrain all bond lengths.

The MD simulations (50000 ps) were performed with a periodic boundary condition in the NPT ensemble at temperature of 0 K to 303.15 K with Berendsen temperature coupling and constant pressure P (1 atm) with isotropic molecule-based scaling. We used a time step of 2 ps and a nonbond interaction cutoff radius of 0.9nm. The average structure, during productive phase, was selected by clustering algorithm method (GROMOS) implemented in Gromacs 4.5.6 software, with 0.2 nm cut-off.

Conflict of interest

The authors confirm that this article content has no conflicts of interest.

Acknowledgments

This work was supported by the National Research Council (CNPq) in Brazil (474386/2012-0). The authors would like to thank the Fundamental Chemistry Department of the Federal University of Pernambuco Brazil for the use of its Analysis Central and Dr. Willian Hunter (University of Dundee) for kindly providing the plasmid with *L. major* PTR1 coding sequence.

References

[1] K.L. Johnston, L. Ford, M.J. Taylor, Overcoming the challenges of drug discovery for neglected tropical diseases: the A·WOL experience, J. Biomol. Screen. 19 (2014) 335–343.

[2] Who, Sustaining the drive to overcome the global impact of neglected tropical diseases, WHO press, Geneva (2012).

[3] T.S. Tiuman, A.O. Santos, T. Ueda-Nakamura, B.P.D. Filho, C. V Nakamura, Recent advances in leishmaniasis treatment, Int. J. Infect. Dis. 15 (2011) 525–532.

[4] A. Marcu, U. Schurigt, K. Müller, H. Moll, R.L. Krauth-Siegel, H. Prinz, Inhibitory effect of phenothiazine- and phenoxazine-derived chloroacetamides on Leishmania major growth and *Trypanosoma brucei* trypanothione reductase, Eur. J. Med. Chem. 108 (2016).

[5] T.T. Guimarães, M.D.C.F.R. Pinto, J.S. Lanza, M.N. Melo, R.L. Do Monte-Neto, I.M.M. De Melo, et al., Potent naphthoquinones against antimony-sensitive and -resistant Leishmania parasites: Synthesis of novel α- And nor-α-lapachone-based 1,2,3-triazoles by copper-catalyzed azide-alkyne cycloaddition, Eur. J. Med. Chem. 63 (2013) 523–530.

[6] R. Pink, A. Hudson, M. Mouriès, M. Bendig, Opportunities and challenges in antiparasitic drug discovery, Nat. Rev. Drug Discov. 4 (2005) 727–740.

[7] M.L. Cunningham, S.M. Beverley, Pteridine salvage throughout the Leishmania infectious cycle: Implications for antifolate chemotherapy, Mol. Biochem. Parasitol. 113 (2001) 199–213.

[8] A.R. Bello, B. Nare, D. Freedman, L. Hardy, S.M. Beverley, PTR1: A reductase mediating salvage of oxidized pteridines and methotrexate resistance in the protozoan parasite Leishmania major, Proc. Natl. Acad. Sci. U.S.A. 91 (1994) 11442–11446.

[9] B. Nare, J. Luba, L.W. Hardy, S. Beverley, New approaches to Leishmania chemotherapy: pteridine reductase 1 (PTR1) as a target and modulator of antifolate sensitivity, Parasitology. 114 (1997) 101–110.

[10] N. Singh, M. Kumar, R.K. Singh, Leishmaniasis : Current status of available drugs and new potential drug targets, Asian Pac. J. Trop. Med. 5 (2012) 485–497.

[11] T.J. Vickers, S.M. Beverley, Folate metabolic pathways in Leishmania, Essays Biochem. 51 (2011) 63–80.

[12] B. Nare, L.W. Hardy, S.M. Beverley, The Roles of Pteridine Reductase 1 and Dihydrofolate Reductase-Thymidylate Synthase in Pteridine Metabolism in the Protozoan Parasite Leishmania major, J. Biol. Chem. 272 (1997) 13883–13891.

[13] L.W. Hardy, W. Matthews, B. Nare, S.M. Beverley, Biochemical and genetic tests for inhibitors of Leishmania pteridine pathways, Exp. Parasitol. 87 (1997) 157–169.

[14] A. Cavazzuti, G. Paglietti, W.N. Hunter, F. Gamarro, S. Piras, M. Loriga, et al., Discovery of potent pteridine reductase inhibitors to guide antiparasite drug development, PNAS. 105 (2008) 1448-1453.

[15] S. Ferrari, F. Morandi, D. Motiejunas, E. Nerini, S. Henrich, R. Luciani, et al., Virtual screening identification of nonfolate compounds, including a CNS drug, as antiparasitic agents inhibiting pteridine reductase, J. Med. Chem. 54 (2011) 211–221.

[16] C. Mendoza-Martínez, J. Correa-Basurto, R. Nieto-Meneses, A. Márquez-Navarro, R. Aguilar-Suárez, M.D. Montero-Cortes, et al., Design, synthesis and biological evaluation of quinazoline derivatives as anti-trypanosomatid and anti-plasmodial agents, Eur. J. Med. Chem. 96 (2015) 296–307.

[17] M.P. Postigo, R.V.C. Guido, G. Oliva, M.S. Castilho, I.R. Pitta, J.F.C. Albuquerque, et al., Discovery of new inhibitors of Schistosoma mansoni PNP by pharmacophore-based virtual screening, J. Chem. Inf. Model. 50 (2010) 1693–1705.

[18] A.A. Bekhit, A.M.M. Hassan, H.A. Abd El Razik, M.M.M. El-Miligy, E.J. El-Agroudy, A.E.D.A. Bekhit, New heterocyclic hybrids of pyrazole and its bioisosteres: Design, synthesis and biological evaluation as dual acting antimalarial-antileishmanial agents, Eur. J. Med. Chem. 94 (2015) 30–44.

[19] H. Nakai, H. Wada, N.T. Meguro, H. Yabana, N-substituted-2-[2-[2-(4-phenylpiper-azine-1-yl)ethoxy]phenyl]-thiazolidine-3-carboxamides useful as cardiotonic agent, U.S.Patent, nº 4,689,327 (1987).

[20] R. Lesyk, B. Zimenkovsky, D. Atamanyuk, F. Jensen, K. Kiec-Kononowicz, A. Gzella, Anticancer thiopyrano[2,3-d][1,3]thiazol-2-ones with norbornane moiety. Synthesis, cytotoxicity, physico-chemical properties, and computational studies, Bioorg. Med. Chem. 14 (2006) 5230-5240.

[21] O. Devinyak, D. Havrylyuk, B. Zimenkovsky, R. Lesyk, Computational search for possible mechanisms of 4-Thiazolidinones anticancer activity: the power of visualization, Molecular Informatics. 33 (2014) 216-229.

[22] S.A.H. El-Feky, Synthesis and anticonvulsant properties of some novel quinazolinone thiazolidine and 4-thiazolidone derivatives, Pharmazie. 48 (1993) 894-896.

[23] R. Ottana, R. Maccari, M.L. Barreca, G. Bruno, A. Rotondo, A. Rossi, et al., 5-Arylidene-2-imino-4-thiazolidinones: design and synthesis of novel anti-inflammatory agents, Bioorg. Med. Chem. 13 (2005) 4243-4252.

[24] R. Maccari, R. Ottanà, R. Ciurleo, M.G. Vigorita, D. Rakowitz, T. Steindl, T. Langer, Evaluation of in vitro aldose redutase inhibitory activity of 5-arylidene-2,4-thiazolidinediones, Bioorg. Med. Chem. Lett. 17 (2007) 3886-3893.

[25] H. Koyama, J.K. Boueres, W. Han, E.J. Metzger, J.P. Bergman, D.F. Gratale, et al., 5-Aryl Thiazolidine-2,4-diones as Selective PPAR Agonists, Bioorg. Med. Chem. Lett. 13 (2003) 1801-1804.

[26] P. Vicini, A. Geronikaki, K. Anastasia, Synthesis and antimicrobial activity of novel 2-thiazolylimino-5-arylidene-4-thiazolidinones. Bioorg. Med. Chem. 14 (2006) 3859-3864.

[27] I.M. Silva, J. Silva Filho, P.B.G.D.S. Santiago, M.S. Egito, C.A. Souza, F.L. Gouveia, et al., Synthesis and Antimicrobial Activities of 5-Arylidene-thiazolidine-2,4-dione Derivatives, Biomed Res. Int. 2014 (2014) 1–8.

[28] T. Tomasic, L.P. Masic, Prospects for Developing New Antibacterials Targeting Bacterial Type IIA Topoisomerases, Current Topics in Medicinal Chemistry. 14 (2014) 130-151.

[29] J.F.C. Albuquerque, C.C. Azevedo, S.L. Galdino, J. Chantegrel, I.R. Pitta, C. Luu-Duc, Synthèse et étude structurale des 5-arilidène thiazolidine-2,4-diones et 4-thio-imidazolidine-2-ones-3-substituées, Ann. Pharm. Fr. 53 (1995) 209-214.

[30] Ö. Bozdag-Dündar, Ö. Özgen, A. Mentes, N. Altanlar, O. Ath, E. Kendi, R.R. Ertana, Synthesis and antimicrobial activity of some new thiazolyl thiazolidine-2,4-dione derivatives, Bioorg. Med. Chem. 15 (2007) 6012–6017.

[31] G. Bruno, L. Costantino, C. Curinga, R. Maccari, F. Monforte, F. Nicolo, R. Ottana, M.G. Vigorita, Synthesis and Aldose Reductase Inhibitory Activity of 5-Arylidene-2,4-thiazolidinedionesy, Bioorg. Med. Chem. 10 (2002**)** 1077–1084.

[32] S.F. Tan, K.P. Ang, Y.F. Fong. (Z)-and (E)-5-Arylmethylenehydantoins: spectroscopic properties and configuration assignment, J. Chem. Soc. 2 (1986) 1941–1944.

[33] M.W. Pantoliano, E.C. Petrella, J.D. Kwasnoski, V.S. Lobanov, J. Myslik, E. Graf, et al., High-density miniaturized thermal shift assays as a general strategy for drug discovery, J. Biomol. Screen. 6 (2001) 429–440.

[34] F.H. Niesen, H. Berglund, M. Vedadi, The use of differential scanning fluorimetry to detect ligand interactions that promote protein stability, Nat. Protoc. 2 (2007) 2212–2221.

[35] G.A. Holdgate, M. Anderson, F. Edfeldt, S. Geschwindner, Affinity-based, biophysical methods to detect and analyze ligand binding to recombinant proteins: Matching high information content with high throughput, J. Struct. Biol. 172 (2010) 142–157.

[36] D. Matulis, J.K. Kranz, F.R. Salemme, M.J. Todd, Thermodynamic stability of carbonic anhydrase: Measurements of binding affinity and stoichiometry using thermofluor, Biochemistry. 44 (2005) 5258–5266.

[37] R.A. Copeland, Assay Considerations for Compound Library Screening. in: R.A Copeland (Ed.), Evaluation of enzyme inhibitors in drug discovery: a guide for medicinal chemists and pharmacologists, Wiley-Interscience, USA, 2005, pp. 82-110.

[38] J. Venkatraman, J. Bhat, S.M. Solapure, J. Sandesh, D. Sarkar, S. Aishwarya, et al., Characterization of mechanistically diverse inhibitors of the Mycobacterium tuberculosis, J. Biomol. Screen. 17 (2012) 293–302.

[39] R.A. Copeland, Reversible Modes of Inhibitor Interactions with Enzymes. in: R.A Copeland (Ed.), Evaluation of enzyme inhibitors in drug discovery: a guide for medicinal chemists and pharmacologists, Wiley-Interscience, USA, 2005, pp. 48-81.

[40] J. Luba, B. Nare, P.H. Liang, K.S. Anderson, S.M. Beverley, L.W. Hardy, Leishmania major pteridine reductase 1 belongs to the short chain dehydrogenase family: stereochemical and kinetic evidence, Biochemistry. 37 (1998) 4093–4104.

[41] A.N. Jain, Surflex: Fully automatic flexible molecular docking using a molecular similarity-based search engine, J. Med. Chem. 18 (2003) 499-511.

[42] D. Van Der Spoel, E. Lindahl, B. Hess, G. Groenhof, A.E. Mark, H.J.C. Berendsen, GROMACS: Fast, flexible, and free, J. Comput. Chem. 26 (2005) 1701–1718.

[43] M.G. Pikkemaat, A.B.M. Linssen, H.J.C. Berendsen, D.B. Janssen, Molecular dynamics simulations as a tool for improving protein stability, Protein Eng. 15 (2002) 185–192.

[44] X. Daura, W.F. Van Gunsteren, A.E. Mark, Folding-unfolding thermodynamics of a β-heptapeptide from equilibrium simulations, Proteins Struct. Funct. Genet. 34 (1999) 269–280.

[45] D. Libermann, J. Himbert, L. Hengl. La thiazolidione, point de depart d'une synthèse des acides thiopyruviques et thioglyoxiliques substituées, Bull. Soc. Chim. Fr. (1948) 1120-1124.

[46] F.L. Gouveia, R.M.B. Oliveira, T.B. Oliveira, I.M. Silva, S.C. Nascimento, K.X.F.R. Sena, et al., Synthesis, antimicrobial and cytotoxic activities of some 5-arylidene-4-thioxo-thiazolidine-2-ones, Eur. J. Med. Chem. 44 (2009) 2038–2043.

[47] A. Dawson, F. Gibellini, N. Sienkiewicz, L.B. Tulloch, P.K. Fyfe, K. McLuskey, et al., Structure and reactivity of Trypanosoma brucei pteridine reductase: inhibition by the archetypal antifolate methotrexate, Mol. Microbiol. 61 (2006) 1457–1468.

[48] Schodinger The PyMOL Molecular Graphics System, Version 1.3, 2009.